Enhanced ability of defect detection using high voltage time-domain resonance analysis and impedance spectrum

Lingfeng Wu,[1] Zhipeng Gao,[2,a)] Kun Yu,[1] Wei Gu,[2] Fuping Zhang,[2] Haiyan Wang,[2] Youcheng Wu,[2] Gaomin Liu,[2] Yujun Feng,[1] Hongliang He,[2] and Xiaoyong Wei[1,a)]
[1]*Electronic Materials Research Laboratory, Key Laboratory of the Ministry of Education & International Center for Dielectric Research, School of Electronic and Information Engineering, Xi'an Jiaotong University, Xi'an 710049, China*
[2]*National Key Laboratory of Shock Wave and Detonation Physics, Institute of Fluid Physics, China Academy of Engineering Physics, Mianyang 621900, China*

(Received 10 January 2018; accepted 22 July 2018; published online 15 August 2018)

Impedance spectroscopy is a well-established method for detecting mechanical defects in materials and structures activated by piezoelectric resonance. However, the detection sensitivity is not always satisfactory for very small defects, such as those that are of great importance for high-field insulation. In this study, an enhanced defect detection method is developed to solve this problem. A high-voltage (1 kV) time-domain resonance analysis is used in combination with conventional impedance spectrum analysis. The resonant frequencies and damping factors of the characteristic high-voltage piezoelectric resonances are extracted from time-domain data, and the damping factors are found to be more sensitive to the defect geometry. The results suggest that the time-domain method used here may have potential for applications where a high sensitivity of defect detection is required. *Published by AIP Publishing*. https://doi.org/10.1063/1.5022079

I. INTRODUCTION

Impedance spectroscopy (IS) is widely used in a variety of applications, such as electrochemical and nondestructive testing.[1] For piezoelectric materials and devices, it is one of the standard methods for the measurement of mechanical and electrical parameters[2] such as capacitance, compliance, coupling factor, and piezoelectric constant. Furthermore, IS can be used to detect mechanical defects in materials and devices. Many such defects have been detected by IS. As early as the 1990s, IS was used to detect bonding defects and cracks.[3] Lim and Soh[4] found that these defects lower the resonant frequency, for example, a 3 mm crack reduces the resonant frequency from 41.4 kHz to 41.1 kHz. Na and Lee[5] studied the effects of partial bonding and full bonding on the impedance and found that partial bonding reduced the impedance from 280 Ω to 240 Ω at the antiresonant frequency but increased it from 190 Ω to 230 Ω at the resonant frequency. Although IS is useful in defect testing, its range of application is still restricted. Most of the detected defects described in the literature are in the millimeter range, and for smaller defects, in the submillimeter range, the change in the impedance spectrum is negligible: as described by Bowen and Lopez-Prieto,[6] there is a difference of only a few ohms at the antiresonant frequency and none at all at the resonant frequency. Thus, it is difficult to test for tiny defects using the conventional IS method.

Gresil *et al.*[7] calculated the effect of the stiffness-proportional damping coefficient on the real part of the impedance. It seems that the damping is more sensitive to defects than the resonant frequency. There have been a number of theoretical studies of the damping at the resonant and antiresonant frequencies.[8–11] Phase angles at the resonant or antiresonant frequency and the impedance values are used to detect defects.[12–16]

Increasing the driving voltage may help to enhance the sensitivity of detection since a larger amplitude of mechanical motion amplifies the interaction between defects and the matrix. However, most of the IS measurement equipment operates at a low signal level of a few volts or at a high voltage and a low frequency (<1 kHz),[17] owing to limitations on output power. To the author's knowledge, there is at present no IS equipment that can operate simultaneously at high voltage (kV) and high frequency (MHz).

To solve this problem, we have developed an experimental setup collecting time-domain signals. Its driving voltage is increased from several volts to a few thousand volts. A pulsed voltage is used corresponding to a frequency range of 1 kHz–1 MHz, which is determined by the test circuit and also by the resonant frequencies of most industrial piezoelectric materials. By analyzing resonance in the time domain, it is possible to detect defects about 0.25 mm in size. The results show that the proposed new method is more effective than conventional IS for detecting defects on a submillimeter scale.

II. EXPERIMENTAL SETUP AND DATA ANALYSIS

Lead zirconate titanate (PZT) ceramic samples of dimensions 16 mm × 16 mm × 3 mm were used in the experiments. One sample, without defects, was denoted state A. In state B, a defect was introduced by using a high-power laser to burn a hole of diameter of about 0.25 mm and a depth of about 0.5 mm on one surface of the ceramic sample. In state C, the laser was used to burn another adjacent hole on the

a)Authors to whom correspondence should be addressed: z.p.gao@foxmail.com and wdy@mail.xjtu.edu.cn

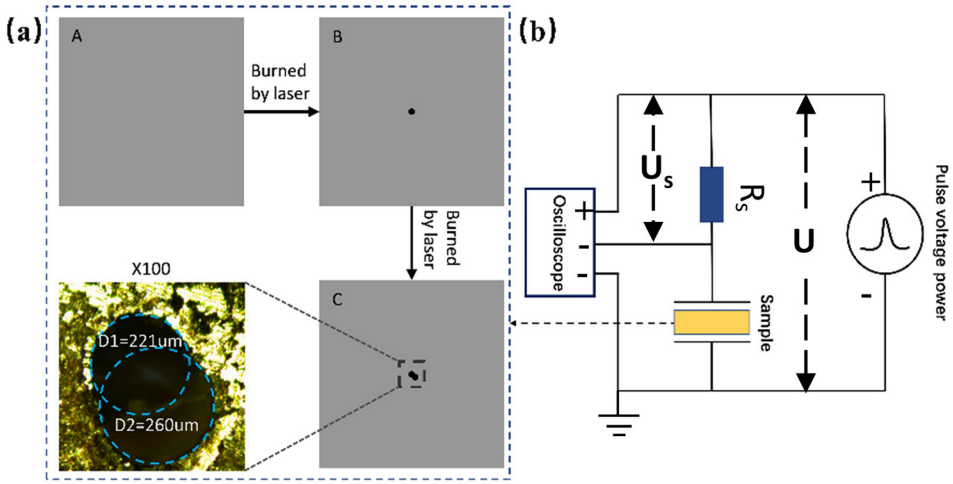

FIG. 1. (a) Sample preparation: the sample with no hole is denoted as state A, the sample with a defect represented by one hole as state B, and the sample with a defect represented by two holes as state C. (b) Diagram of the test circuit.

surface of the ceramic sample, again each of approximate diameter 0.25 mm and depth 0.5 mm. Figure 1(a) shows a schematic diagram of the three samples and a magnified image of state C. The test circuit is shown in Fig. 1(b).

The high-voltage power source generated pulsed voltages with a rise time of 1 μs and a maximum voltage reaching 10 kV. A resistance of 56 kΩ was used to measure the current. An oscilloscope (Lecroy 606zi) was used to record time-domain voltage and current data.

The total voltage U was collected directly, and the current I was calculated as U_s/R_s. Using the Fourier transform, the voltage and current data in the time domain can be transferred into the frequency domain

$$Z(iw) = \frac{U(iw)}{I(iw)} = \frac{F[U(t)]}{F[I(t)]}. \tag{1}$$

In principle, an impedance spectrum can be calculated using Eq. (1). However, given the limits imposed by the accuracy of the test and the effective test time, the accuracies of the frequency and the phase calculated by the Fourier transform are not sufficient. To obtain a more accurate result, we use an equivalent circuit to analyze the data further. The equivalent circuit for one-dimensional vibration is shown in Fig. 2.[18] The component C_0 represents the static capacitance, while R_1, L_1, and C_1 represent the dynamic resistance (damping), dynamic inductance, and dynamic capacitance, respectively. These dynamic components are related to piezoelectric vibration.

Based on this equivalent circuit, the time-domain current satisfies the following equation:

$$I(t) = I_0 e^{-\sigma_0 t} + I_1 e^{-\sigma_1 t}\cos(2\pi f_1 t + \varphi_1), \tag{2}$$

where

$$\sigma_1 = \frac{R_1}{2L_1}. \tag{3}$$

The two terms on the right-hand side of Eq. (2) correspond to the discharge current of the static capacitor C_0 and an underdamping resonance of the *RLC* circuit. By fitting the time-domain data using Eq. (2), we can evaluate the values of the parameters in this equation. The damping factor σ_1, which, as shown in Eq. (3), is proportional to the dynamic resistance R_1, can then be obtained and will reflect the change in damping.

There are three clear resonances for our samples. Thus, the complete expression for the current should take the following form:

$$I(t) = I_0 e^{-\sigma_0 t} + I_0 e^{-\sigma_1 t}\cos(2\pi f_1 t + \varphi_1) + I_2 e^{-\sigma_2 t}\cos(2\pi f_2 t + \varphi_2) + I_3 e^{-\sigma_3 t}\cos(2\pi f_3 t + \varphi_3). \tag{4}$$

It is easy to obtain the resonant frequencies f_1, f_2, and f_3 and the damping factors σ_0, σ_1, σ_2, and σ_3 of each sample by fitting the data to Eq. (4).

III. RESULTS AND DISCUSSION

The voltage and current data in the time domain collected by the oscilloscope are presented in Fig. 3(a), which shows a typical capacitor charging process plus small disturbance signals [as can be seen in the magnified plot in Fig. 3(b)], which are caused by piezoelectric vibrations. We can see these vibrations more clearly in the results of Fourier

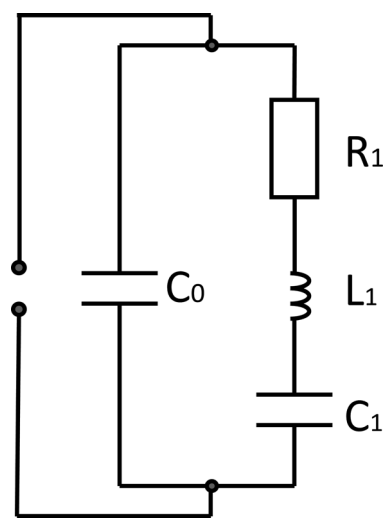

FIG. 2. Equivalent circuit of a ceramic when only one-dimensional vibrations are considered.

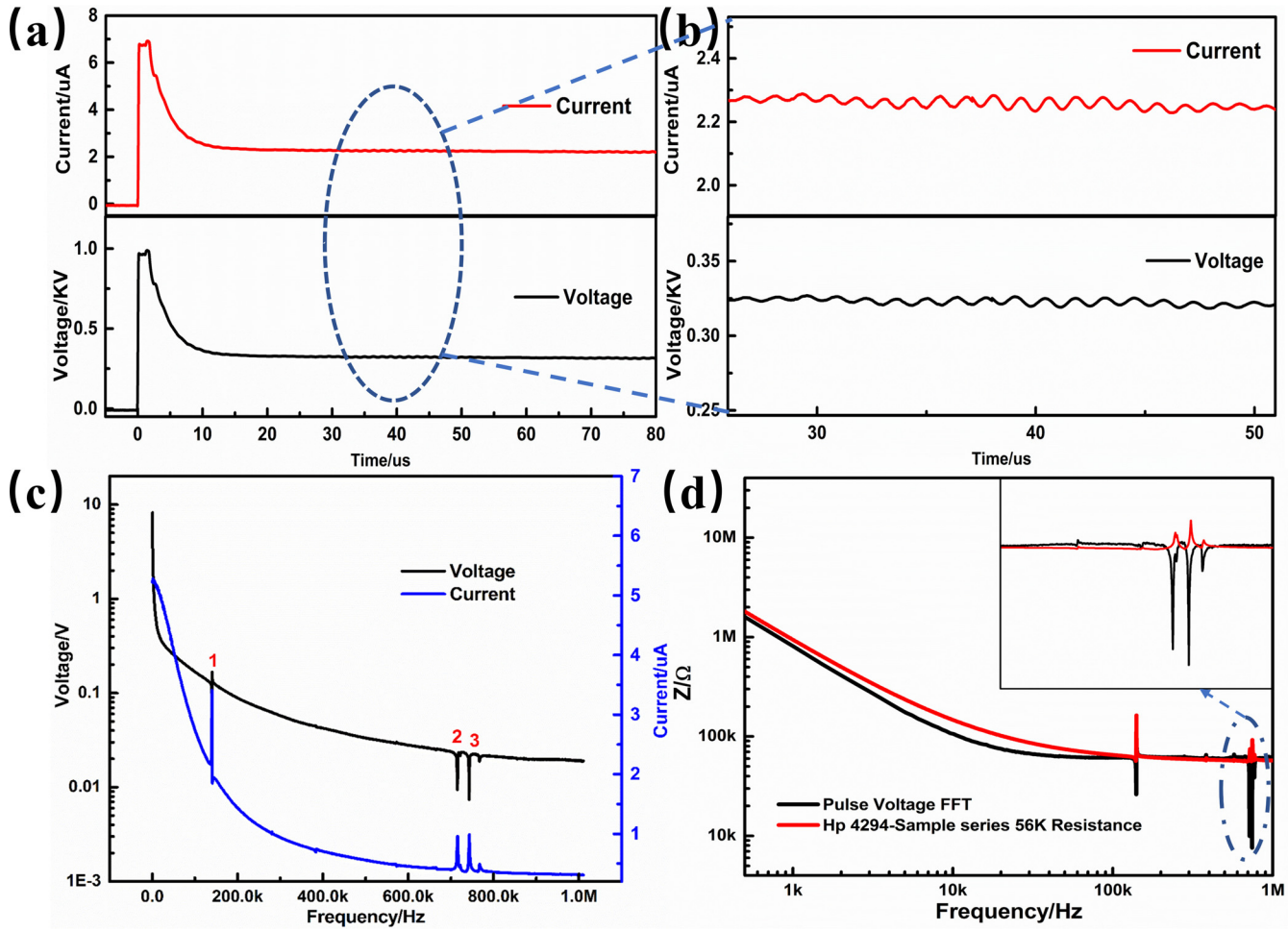

FIG. 3. (a) Original test results. (b) Oscillations in the original data. (c) Fourier transforms of voltage and current. (d) Impedance calculated using Eq. (1) and obtained directly with an HP 4294 impedance analyzer.

transformation presented in Fig. 3(c). Both the voltage and current in the frequency domain have three peaks, and similar peaks can also be seen in the results of a normal IS test shown in Fig. 3(d). Therefore, it is obvious that the peaks in Fig. 3(c) are due to mechanical resonances of the sample. We can also calculate the impedance value using Eq. (1), which gives the results shown in Fig. 3(d). These calculated values are very close to those obtained directly using a conventional small-signal HP 4294 impedance analyzer (Hewlett Packard) with a 56 kΩ serial resistance. This excellent match proves that the time-domain method can detect piezoelectric resonance, as observed by Jin *et al.*[19] in PZT ceramics. However, owing to limits on the effective test time and the test accuracy, more accurate results for the frequency and phase are difficult to obtain.

The finite element method[20] is an effective way to analyze vibrational modes. Figure 4 illustrates the modal analysis associated with three modes at frequencies 140 kHz, 714 kHz, and 743 kHz. These three frequencies are in accord with the frequencies of the peaks observed in Fig. 3(c). The modes at 140 kHz and 714 kHz are extension vibrations in the lateral direction (16 mm) and the thickness direction (3 mm), respectively, while the mode at 743 kHz is a coupling mode between the thickness resonance and a distortion mode.

By fitting the time-domain current data using Eq. (4), it is possible to improve the accuracy of the resonant frequencies

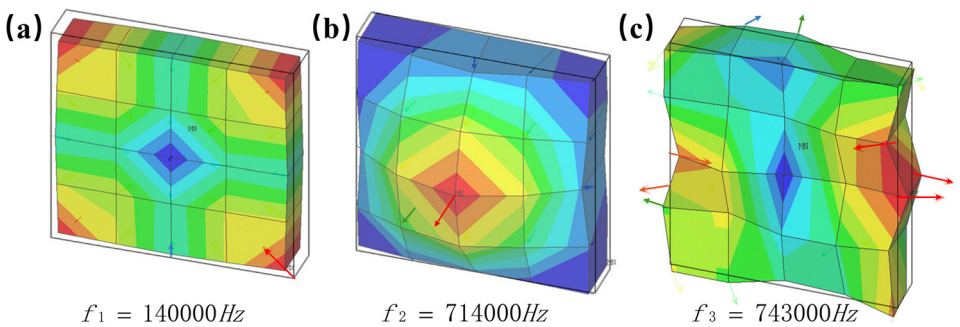

FIG. 4. Structural vibrational modes at three resonant frequencies: (a) extension resonance mode in the lateral direction, (b) extension resonance mode in the thickness direction, and (c) coupled distortion mode.

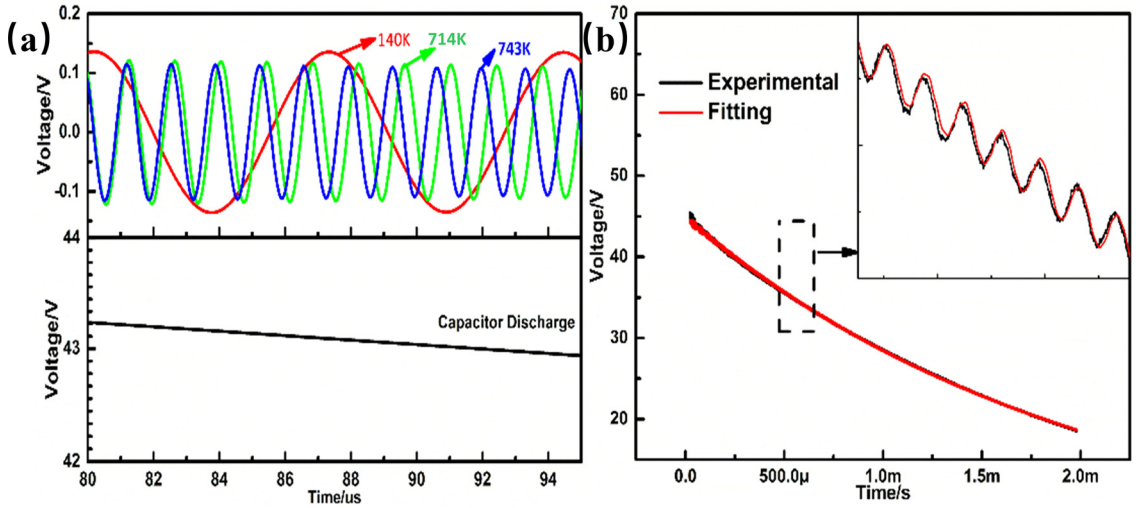

FIG. 5. (a) Fitting procedure with the initial date being filtered into four parts. (b) Fitted results.

TABLE I. Main parameters measured by the HP 4294 impedance analyzer and obtained by data fitting.

	Measured by Hp4294						Obtained by data fitting					
	Resonant frequency			Maximum value of phase angle			Resonant frequency			Damping factor		
Sample	f_1 (kHz)	f_2 (kHz)	f_3 (kHz)	θ_1 (°)	θ_2 (°)	θ_3 (°)	f_1 (kHz)	f_2 (kHz)	f_3 (kHz)	σ_1	σ_2	σ_3
State A	140.0	714.6	743.6	71.7	86.8	75.8	140.3	714.8	743.2	892 ± 0.6	8204 ± 31	8520 ± 32
State B	140.0	714.6	743.6	69.2	86.2	74.7	140.2	714.2	742.6	903 ± 0.7	10070 ± 37	8610 ± 34
State C	139.9	714.6	743.5	68.2	86.1	74.3	140.2	713.9	741.8	910 ± 0.7	11790 ± 39	8630 ± 34

and damping factors. As shown in Fig. 5(a), the initial data can be filtered into four parts, the first of which is capacitor discharge, while the other three are oscillating attenuations, each representing a vibration of the sample. The fitted results are shown in Fig. 5(b). There is a perfect match between the fitted results and the original data.

We have now obtained three resonant frequencies of the sample from fitting the data. The three frequencies f_1, f_2, and f_3 and the maximum values of the phase angles θ_1, θ_2, and θ_3 measured by the HP 4294 impedance analyzer and those obtained by data fitting are listed in Table I. The defects (i.e., the holes burned by the laser) decrease the resonant frequencies and the phase angles. However, the maximum decrease in the resonant frequencies is less than 2 kHz, and the decrease in the maximum values of the phase angles never exceeds 3°. We cannot effectively detect defects through changes in either the frequencies or the phase angles. However, the damping factors of the samples in the three states are very different. We can see these differences in Fig. 6(b). There are four damping factors σ_0, σ_1, σ_2, and σ_3 in Eq. (4). Three of them change only slightly, whereas σ_2 changes considerably, with values of 8204, 10 070, and 11 790 in the three states. It seems that the defects in the ceramic cause an increase in this damping factor. This change in σ_2 is sufficiently large to allow its use to identify defects.

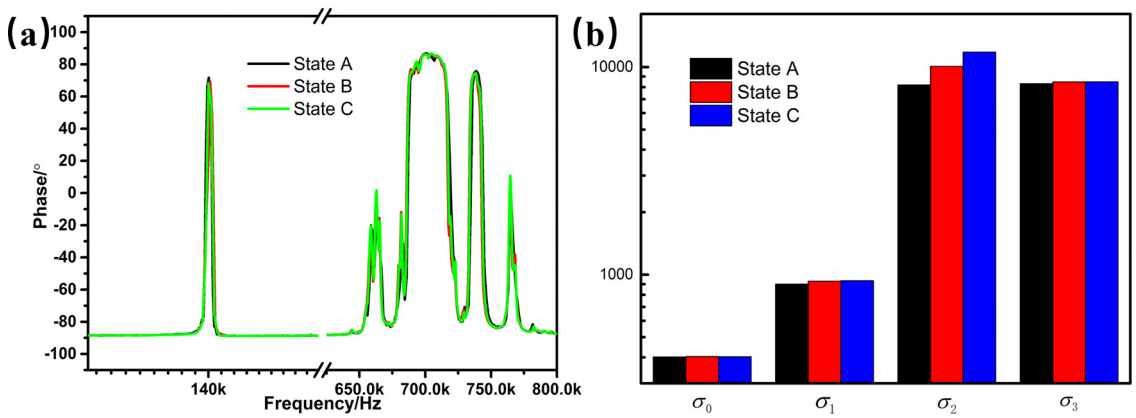

FIG. 6. Comparison of the samples in the three states: (a) phase angles measured by the HP 4294 impedance analyzer and (b) damping factors.

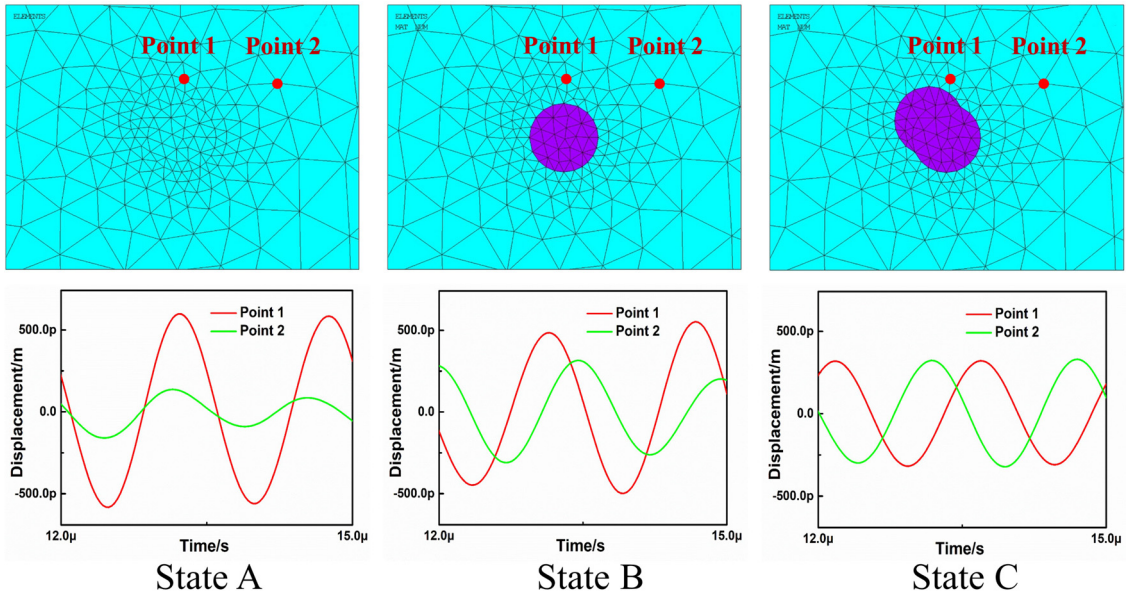

FIG. 7. Top row: Finite element transient analysis. Bottom row: Displacements of points 1 and 2 excited by a sinusoidal signal in the three states.

The dynamic resistance in the equivalent circuit represents a heat loss in the physical system. In our experiments, heat loss is mainly caused by internal friction. An increase in a damping factor implies an increase in internal friction. We suggest that the vibrational modes of the sample are changed by the defects. These modes change from homogeneous vibrational modes to distorted modes, which leads to increases in the relative displacements between the various parts of the samples.

The three states of the ceramic sample meshed by the finite element method are shown in the top row of Fig. 7. There is no defect in state A, while cylindrical holes representing the defects are introduced in states B and C. Through modal analysis, the movements of the points of the mesh are extracted at a resonant frequency near 714 kHz, corresponding to σ_2. Two points are marked in the model. We can subject the model to a voltage load at the resonant frequency. The relative displacement of the two points can then be calculated by transient analysis. The relative displacement is used to illustrate the effect of the defects on internal friction. The results are shown in the bottom row of Fig. 7. In state A, where there is no defect in the sample, the directions of vibration of points 1 and 2 are the same, and the relative displacement is minimal. In states B and C, the directions of vibration of points 1 and 2 are different, with the phase difference in state C being larger than that in state B. This means that the presence of a defect can lead to an increase in heat loss. Therefore, the defect will cause an increase in the damping factor.

IV. CONCLUSIONS

An enhanced method for detection of defects has been developed using high-voltage pulses as pumping signals in time-domain resonance analysis. Using this new method, we can calculate the impedance spectrum of detected defects from 1 kHz to 1 MHz under a high voltage of up to several kilovolts. The resonant frequencies and damping factors of characteristic high-voltage piezoelectric resonances have been extracted from voltage and current data, and the damping factor has been found to be more sensitive to defect geometry since defects may cause internal friction and heat loss, as demonstrated by finite element analysis. These results convince us that the time-domain method used here may have potential for applications requiring a high sensitivity of defect detection.

ACKNOWLEDGMENTS

This work was supported by the National Basic Research Program of China (No. 2015CB654602), the International Science and Technology Cooperation Programs of China (No. 2015DFA51100), NSFC Projects (No. 51761145024), the Shanxi Province Project (No. 2017ktpt-21, 2018TD-024), the 111 Project (No. B14040), the LSD fund (Grant No. 6142A03010102), the LSD engineering project (Grant No. 2016Z-04), the Dean Fund of CAEP (Grant No. YZJJLX2016001), the CSS project (Grant No. YK2015-0602006), and the National Natural Science Foundation of China (Grant No. 11704353).

[1]E. Barsoukov, *Impedance Spectroscopy: Theory, Experiment, and Applications* (Wiley, New York, 2005).
[2]T. Takagi, M. Uesaka, and K. Miya, *Electromagnetic Nondestructive Evaluation* (IOS Press, 1997), Vol. 12, p. 9.
[3]R. D. Adams and B. W. Drinkwater, NDT&E Int. **30**, 93 (1997).
[4]Y. Y. Lim and C. K. Soh, Smart Mater. Struct. **20**, 125001 (2011).
[5]S. Na and H. K. Lee, Compos. Struct. **94**, 2383 (2012).
[6]C. R. Bowen and M. Lopez-Prieto, Scr. Mater. **42**, 6 (2000).
[7]M. Gresil, L. Y. Yu, V. Giurgiutiu, and M. Sutton, Struct. Health Monit. **11**, 671 (2012).
[8]K. Uchino and S. Hirose, IEEE Trans. Ultrason. Ferroelectr. Freq. Control **48**, 307 (2001).
[9]T. Tsurumi, H. Kakemoto, and S. Wada, in *ISAF 2002: Proceedings of the 13th IEEE International Symposium on Applications of Ferroelectrics* (IEEE, New York, 2002), p. 375.
[10]T. Tsurumi, M. Shono, H. Kakemoto, S. Wada, K. Saito, and H. Chazono, Jpn. J. Appl. Phys. **44**, 6989 (2005).
[11]Y. Zhuang, S. O. Ural, A. Rajapurkar, S. Tuncdemir, A. Amin, and K. Uchino, Jpn. J. Appl. Phys. **48**, 041401 (2009).

[12]M. E. Ebrahimi, J. Chevalier, and G. Fantozzi, J. Mater. Res. **15**, 142 (2000).
[13]K. Kaneda, S. Lee, N. J. Donnelly, W. G. Qu, C. A. Randall, and Y. Mizuno, J. Am. Ceram. Soc. **94**, 3934 (2011).
[14]A. Tiefenbach and B. Hoffmann, J. Eur. Ceram. Soc. **20**, 2079 (2000).
[15]S. Ritdumrongkul and Y. Fujino, Struct. Control Health Monit. **14**, 931 (2007).
[16]K. Prabakar and S. P. M. Rao, J. Alloys Compd. **437**, 302 (2007).
[17]M. Shi, *AC Impedance Spectroscopy: Principles and Applications* (National Defense Industry Press, Beijing, 2001).
[18]C. Wang and M. Zhao, *Piezoelectric Ferroelectric Physics* (Press of Science and Technology, Beijing, 2009).
[19]L. Jin, X. Yao, X. Y. Wei, and Z. Z. Xi, Appl. Phys. Lett. **87**, 082905 (2005).
[20]T. Belytschko, R. Gracie, and G. Ventura, Modell. Simul. Mater. Sci. Eng. **17**, 043001 (2009).